

## Coupled Analysis of Unsteady Aerodynamics and Vehicle Motion of a Passenger Car in Crosswind Condition

T. M. Huang<sup>1,2†</sup>, Z. Q. Gu<sup>1,3</sup> and C. J. Feng<sup>1</sup>

<sup>1</sup>State Key Laboratory of advanced Design and Manufacturing for Vehicle Body, Hunan University, Changsha 410082, P. R. China

<sup>2</sup>Hunan Institute of Science and Technology, Yueyang 414000, P.R. China

<sup>3</sup>Hunan University of Arts and Science, Changde 415000, P.R. China

†Corresponding Author Email: [htm426@hnu.edu.cn](mailto:htm426@hnu.edu.cn)

(Received June 5, 2016; accepted October 27, 2016)

### ABSTRACT

High-speed passenger car requires a lighter weight for improving power performance and reducing fuel consumption; a car with higher-speed and lighter weight will lead to the passenger car more sensitive to the crosswind, which will affect the stability and drivability of the passenger car. This study employs the fully-coupled method to investigate a passenger car subjected “1-cos” crosswind with consideration of the vehicle motion. Large eddy simulation (LES) and dynamic mesh is adopted to investigate the unsteady aerodynamic, and the vehicle is treated as a three-freedom-system and driver’s control is considered to investigate the vehicle dynamic. The one-way simulation and quasi-steady simulation are also conducted to compare with the fully-coupled simulation. The results of the three simulation methods show large difference. The peak value of the lateral displacement in fully-coupled simulation is the smallest between the three simulation approaches. While the change of aerodynamic loads and vehicle motion in fully-coupled simulation is more complicated than in one-way and quasi-steady simulation. These results clearly indicate the significance of including of the unsteady aerodynamic loads in passenger car moving analysis.

**Keywords:** Unsteady aerodynamic; Large-eddy simulation; Vehicle motion; Fully-coupled simulation; One-way simulation; Quasi-steady simulation.

### NOMENCLATURE

$C_{sm}$	Smagorinsky constant	$\bar{P}$	filtered pressure
$C_s$	lateral force coefficient	$S$	windward area
$C_{ym}$	yawing moment coefficient	$S_{ij}$	strain rate tensor
$C_d$	drag force coefficient	$T_{ij}$	aligning torque
$C_l$	lift force coefficient	$\bar{u}_i$	filtered velocity
$d$	front and rear wheel track	$u$	passenger car velocity in longitudinal direction
$F_w$	aerodynamic lateral force acting on the car	$v$	passenger car velocity in lateral direction
$F_{s,y}$	crosswind lateral force on passenger car	$v_s$	crosswind velocity
$F'_{x_y}$	tire forces in longitudinal direction	$V$	volume of the computational cell
$F'_{y_y}$	tire forces in lateral direction	$V_r$	relative velocity of the car
$H$	height	$W$	width
$I_z$	moment of inertia	$y^+$	wall normal distance
$L_s$	length for subgrid-scales	$y_{t_0+t_p}$	prediction displacement of the vehicle
$l_f$	the distance from gravity center to front wheel	$\nu$	kinematic viscosity
$l_r$	the distance from gravity center to rear wheel	$\delta_{rad}$	driver’s feedback to the vehicle routing
$L$	length	$\delta_{Lw}$	driver’s reaction to the crosswind
$M_{w,z}$	crosswind yawing moment acting on passenger car	$\beta_w$	aerodynamic yaw angle
$m$	mass	$\theta$	yaw angle of the passenger car
		$\delta$	steering angle of the front tire

$\rho$	air density	$\tau_{ij}$	residual stresses
$\tau$	time delay of the driver reaction		
$K$	von Karman constant		

## 1. INTRODUCTION

Crosswind stability and drivability of high-speed road vehicle has attracted more and more attention during the last decades, in order to promote vehicle aerodynamic design and technology to a higher level. Crosswind may threaten the safety of the running vehicle due to the unsteady aerodynamic loads (Cai 2015). Many reports (Wang *et al.* 2014) show that the crosswind is a significant factor causing the vehicle accidents.

In the past several decades, a number of experimental studies have been conducted on road vehicle aerodynamics under crosswind condition (Wang *et al.* 2014; Li *et al.* 2014; Chu *et al.* 2013; Tosolin *et al.* 2013). Based on the report of experimental researches it could be found that the aerodynamic loads acting on the vehicle appears obvious unsteadiness under a sudden crosswind. However, the experiment approaches under some conditions are bounded due to their inherent limitations (Okada *et al.* 2009). Adopting complex test rig or advanced test methods for experiment is very complex and difficult to achieve. Besides, drive test or wind tunnel measurement provides very limited flow information about the test. The lack of flow information could restrain detailed flow analysis which is needed to understand the physical mechanism. Hence, the computational fluid dynamics (CFD) becomes a valuable alternative and provides insights into overcoming the limitations of experiments. Since the flow filed around the vehicle is unsteadiness when the vehicle driving on road, the time-dependent method such as LES, should be employed to obtain instantaneous information about the flow filed. Some researches on unsteady aerodynamics of road vehicle using LES show that the LES could obtain the transient flow features around the vehicle (which is difficult to get by RANS) with good agreement with the corresponding experimental results (Uystepuyst *et al.* 2013; Gulyasa *et al.* 2013; Jonathan *et al.* 2015). Hence in this study, the LES is utilized to investigate the unsteady crosswind aerodynamics.

The stability and drivability of road vehicle under crosswind condition have been investigated during the past decades. However, most of the study only consider the effect of unsteady aerodynamics to the stability and drivability of the vehicle, and the effect of vehicle motion to the aerodynamics is not included. For instance, Wang and Xu (2015) investigated a truck passing by a bridge tower under crosswind condition, but the aerodynamics loads are first obtained in terms of time-varying aerodynamics loads from CFD simulations. The results imply that the rolling and lateral motions of the truck are affected obviously by the tower. Nakashima *et al.* (2011) adopted the steady and quasi-steady aerodynamics loads coupling vehicle

motion to study the vehicle performance in wind gusts condition. The results show that the rolling motion is affected by both the aerodynamics load and the lateral motion of the truck.

Though these researches show some important aspects, it is still difficult to mimic the real driving condition accurately. Since the vehicle motion and unsteady aerodynamics are interplayed with each other during real road driving. Therefore, it will be interesting to investigate the vehicle motion coupled with the unsteady aerodynamics. The fully-coupled simulation method could help to understand the change of the aerodynamic characteristics, the route deviation of the vehicle and the driver's reaction more clearly. However, very few studies can be found in the area of coupling effect study of vehicle motion and unsteady aerodynamics so far. Cui *et al.* (2014) investigated the safety conditions of high-speed trains subjected to crosswind while the change of the train's posture was considered. The results showed the safety domain decreases due to the influence of the posture change to the aerodynamic force. Zhou and Chen (2015) investigated the driving safety of the moving vehicle on bridge subjected crosswind by fully-coupled method, the results showed the vehicle is more possible to be lifted up or slip laterally. Nevertheless, crosswind stability is the result of complex interactions between aerodynamics, vehicle dynamics and the driver. But the studies mentioned above did not consider the driver's reaction, which is very important for realistic driving vehicle. Some researchers have proposed driver reaction model on crosswind condition. For example, Maruyama and Yamazaki (2006), Baker (1988), Manfred and Henning (2003) and so on. Nakashima *et al.* (2013) investigated truck in crosswind condition with the driver model proposed by Maruyama (2006) by fully-coupled simulation method. The results shown the driver's reaction is very important. Moreover, it has to be noted that the study objects mentioned above are mainly focus on the train or truck, which is different for passenger car. As the requirement of improve power performance and reduce fuel consumption, the stability and drivability of the passenger car become more susceptible than other types vehicle to the unsteady aerodynamics loads. The influence of the unsteady aerodynamics load to the passenger car should be considered when the passenger car drives on road.

The present study aims to investigate the stability and drivability of a passenger car in crosswind condition by fully-coupled, quasi-steady and one-way simulation method with LES, and the driver reaction model proposed by Manfred sand Henning (2003) is used in the study. It will analyze the difference between the results of the three methods and evaluate the passenger car performance in

crosswind condition.

The paper is organized as follows: the passenger car model is presented in second section, the governing equation is presented in third section, the simulation method numerical methods, and experimental are presented in fourth section. The results are presented and discussed in the fifth section. Finally, the sixth section is the conclusion.

## 2. TARGET PASSENGER CAR

The target passenger car in the present study is a simplified passenger car model which is based on the real commercial passenger car, with its length, width and height of 4587mm, 1762mm, and 1468mm, respectively. Fig. 1 shows the orthogonal view of the simplified passenger car geometry. Some details are removed, such as side mirrors, wiper, air-inlet grill and so on, and the body surface is smoothed to reduce the computational effort of the coupled simulation of the unsteady aerodynamics and passenger car's motion.

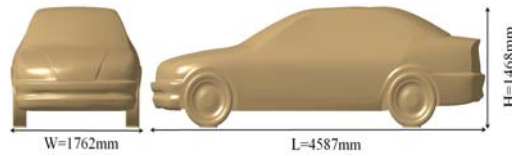


Fig. 1. Passenger car model.

## 3. GOVERNING EQUATION

### 3.1 Fluid Dynamics

The filtered continuity and momentum equations read

$$\frac{\partial \bar{\rho}_i}{\partial x_i} = 0 \quad (1)$$

$$\frac{\partial \bar{u}_i}{\partial t} + \frac{\partial \bar{u}_i \bar{u}_j}{\partial x_j} = -\frac{1}{\rho} \frac{\partial \bar{P}}{\partial x_i} + \nu \frac{\partial^2 \bar{u}_i}{\partial x_j \partial x_j} - \frac{\partial \tau_{ij}}{\partial x_j} \quad (2)$$

where  $\bar{u}_i$  is the filtered velocity,  $\rho$  represents the air density,  $\bar{P}$  stands for the filtered pressure,  $\nu$  is the kinematic viscosity, and  $\tau_{ij}$  is the residual stresses.

The residual stresses are unknown and need to be modeled. The linear eddy viscosity model is used to relate the subgrid stresses to the resolved strain-rate tensor  $\bar{S}_{ij}$  as

$$\tau_{ij}^R - \frac{1}{3} \tau_{kk} \delta_{ij} = -2\nu_{SGS} \bar{S}_{ij} = -\nu_{SGS} \left( \frac{\partial \bar{u}_j}{\partial x_i} + \frac{\partial \bar{u}_i}{\partial x_j} \right)$$

The Smagorinsky-Lilly model is used for SGS turbulent viscosity

$$\nu_{SGS} = \rho L_s^2 |\bar{S}| = \rho L_s \sqrt{2 \bar{S}_{ij} \bar{S}_{ij}}$$

where  $L_s = \min(\kappa d_s, C_{sm} V^{\frac{1}{3}})$

$L_s$  is the mixing length for subgrid-scales.

$\kappa$  denotes the Vo Karman constant.  $d_s$  represents the distance to wall and  $V$  is the volume of the computational cell.  $C_{sm}$  is the Smagorinsky constant, which is set as 0.1 in this study (Zhu 2015).

Equations (1) and (2) are discretized using 3D finite volume method for solving the incompressible N-S equations. The convergence criterion of the residual of continuity, momentum and energy equations is set to be  $10^{-5}$ . A second-order conservative scheme is used to approximate the convective fluxes, for the spatial derivative. The time-dependent terms of the equations are interpolated by the second order implicit scheme. The coupling between pressure and velocity in momentum equation is implemented by SIMPLE algorithm, which was shown by Liu *et al.* (2016).

## 3.2 Vehicle Dynamics

### 3.2.1 Motion Equation

To simplify the problem, the passenger car is assumed to compose by the upper body and tires. The passenger car body is treated as a rigid body. The passenger car is not moving in vertical direction, and the pitching and rolling motion is not considered, which means the passenger car only move in horizontal direction. Based on the assumption, the passenger car is assumed as a three-degree-freedom system. A similar system has been verified by Maruyama *et al.* (2006). The coordinate system of the passenger car model for dynamic simulation is assumed to be the gravity center which is taken as the real commercial passenger car as shown in Fig. 2.

Based on the above hypothesis, the governing equations of the passenger car dynamic model are expressed as follow,

$$m \left( \frac{du}{dt} - v \frac{d\theta}{dt} \right) = \sum_i \sum_j (F_{x_{ij}} \cos \delta - F_{y_{ij}} \sin \delta) F'_{x_{ij}} = \sum_{i,j} F'_{x_{ij}} \quad (3)$$

$$m \left( \frac{dv}{dt} - u \frac{d\theta}{dt} \right) = \sum_i \sum_j (F_{x_{ij}} \sin \delta + F_{y_{ij}} \cos \delta) + F_{s,y} = \sum_{i,j} F'_{y_{ij}} + F_{s,y} \quad (4)$$

$$I_z \frac{d^2 \theta}{dt^2} = (F'_{y_{11}} + F'_{y_{12}}) l_f + (F'_{x_{11}} - F'_{x_{12}}) \frac{d}{2} - (F'_{y_{21}} + F'_{y_{22}}) l_r + (F'_{x_{21}} - F'_{x_{22}}) \frac{d}{2} + M_{\omega z} + \sum_i \sum_j T'_{ij} \quad (5)$$

Where  $u$  is the passenger car velocity in longitudinal direction, and  $v$  is the passenger car velocity in lateral direction.  $\theta$  is the yaw angle.  $\delta$  is the steering angle of the front tire.  $F'_{x_{ij}}$  depends on the loading and speed ratio between the tire rotation velocity and the passenger car velocity.

However, the velocity of the passenger car in X-direction is not influenced by the driver due to the driver is assumed only to control the steering. Hence,  $F_{x_{ij}}$  is set as a constant value.  $T_{ij}$  and  $F_{y_{ij}}$  are influenced by the side slip angle and loading on the tire. The Magic Formula Model (Bakker 1989) is adopted to calculate the tire force and the aligning torque in this study.

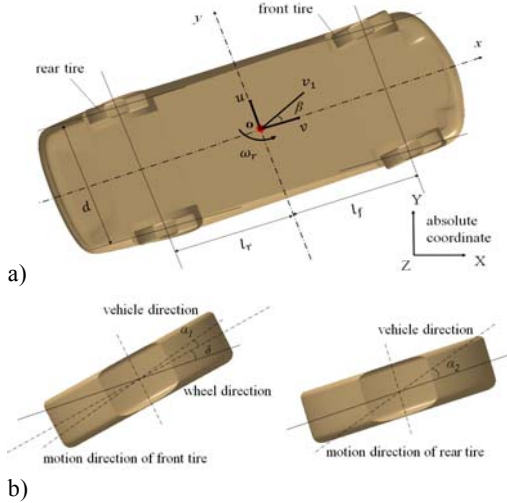


**Fig. 2. Coordinate of the passenger car model.**  
a) body; b) tires.

### 3.2.2 Driver Reaction Model

In order to regenerate the driver's reaction when the passenger car deviate the route, the driver model proposed by Manfred and Henning (2003) which is utilized to reappear the steering action of the driver. The steering angle  $\delta$  is composed by  $\delta_{LW}$  and  $\delta_{road}$ .  $\delta_{LW}$  denotes the driver's reaction to the crosswind and  $\delta_{road}$  stands for the driver's feedback to the vehicle routing.

$\delta_{LW}$  is showed as follow,

$$\delta_{LW} = \begin{cases} 0 & 0 \leq t \leq 0.8 \\ \delta_{wind}(1 - e^{-0.7(t-0.8)}) & 0.8 \leq t \leq 2.8 \\ 0 & 2.8 \leq t \leq \infty \end{cases} \quad (6)$$

$\delta_{road}$  is expressed as follow

$$\delta_{road} = -0.0975 \times 15 y_{t_0+t_p} \quad (7)$$

The steering angle  $\delta$  is an input to the model as follow,

$$\delta = \begin{cases} \delta_{road} & 0 \leq t \leq 0.8 \\ \delta_{wind}(1 - e^{-0.7(t-0.8)}) + \delta_{road} & 0.8 \leq t \leq 2.8 \\ \delta_{road} & 2.8 \leq t \leq \infty \end{cases} \quad (8)$$

Where  $\delta_{wind}$  is set to 0.306.  $\tau$  shows the time delay

of the driver reaction, and the value is 0.3s in this study.  $y_{t_0+t_p}$  is the prediction displacement of the vehicle after  $t_p$  second.

## 4. NUMERICAL SETUP

### 4.1 Fluid Dynamic Simulation

#### 4.1.1 Boundary Condition

The shape of the computational domain is set as a rectangular duct as shown in Fig 3. The rectangular duct has a length of  $20L$ , width of  $33W$  and height of  $10H$ , with the passenger car located on the floor. This set up produces a small blockage ratio about 0.25%, which is well within the accepted range of 5% in vehicle aerodynamic simulation (Hucho and Sovran 1993). The passenger car is located approximately  $5L$  downstream of the main inlet boundary plane in front of the passenger car.

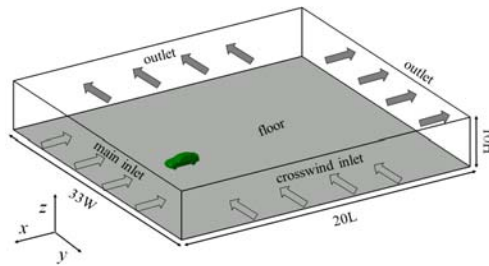


**Fig. 3. Computation domain.**

The '1-cos' crosswind is used in this study. The type of '1-cos' shape could be used to approximate unsteady aerodynamic loads on vehicle (Carrarini 2006). Fig. 4 presented the profile of the crosswind velocity. The crosswind is appeared from  $t=0.5s$  to  $t=2.5s$ , and the peak value of the crosswind is set to  $-15m/s$ .

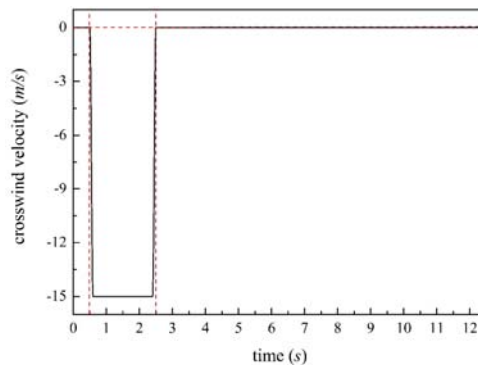


**Fig. 4. Crosswind velocity profile.**

At the main inlet boundary, the air flow is set to be a constant velocity of  $-30m/s$ , which donates the velocity of passenger car. The '1-cos' crosswind as shown in Fig 4 is imposed on the crosswind inlet boundary. The upstream turbulence intensity is 0.5%, and the turbulent viscosity ratio is 10. Pressure-outlet condition is used on the outlet boundary. The passenger car body surface is treated

**Table 1 Detailed grid size tests and experiment**

Data	Case 1	Case 2	Case 3	Case 4	Case 5	experiment
Number of cells	28532168	24013569	21156237	17962513	16856128	
$Cd$	0.285	0.285	0.287	0.291	0.296	0.284
$Cl$	-0.048	-0.048	-0.051	-0.055	-0.060	-0.047

as no-slip wall condition, and the roof of the domain is set as free-slip wall condition.

$$v_s = \begin{cases} 0 & 0 < t < 0.5 \\ -15(1 - \cos 5(t - 0.5)\pi) & 0.5 \leq t < 0.6 \\ -15 & 0.6 \leq t < 2.4 \\ -15(1 - \cos 5(t - 2.5)\pi) & 2.4 \leq t < 2.5 \\ 0 & 2.5 \leq t \end{cases}$$

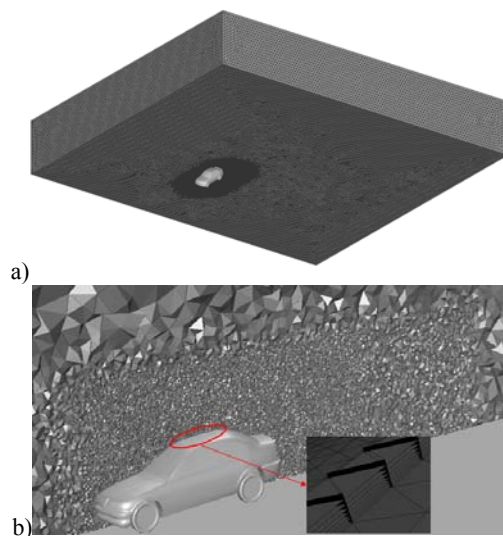


**Fig. 5. a) Computational grid topology; b) boundary layer.**

#### 4.1.2 Computational Grid

The grids are constructed by using the software Ansys ICFM-CFD in this study. The grid topology is divided into several blocks in spatial resolution to obtain more information of the flow-field around the passenger car and reduce the simulation effort as shown in Fig 5. Accordingly, the finest block is the boundary layers, which is created with 8 prism mesh layers, and the growth rate is 1.15. The mesh of the prism layer is comprised by triangular prism cells. The size of the grid adjoining to passenger car body must be small enough to disintegrate the flow structure in the viscous area of the boundary layer, which require  $y^+$  smaller than 10 (Osth and Krajnovic 2013). The  $y^+$  is around 1.0 in this study. The resolution in the streamwise direction is about 5, and the resolution in directions normal to spanwise is about 6. Next to the prism layers is the second-finest region, which aims to capture more details of flow structures around the passenger car. The third-finest region is located downstream of the passenger car to gain more information about the

wake flow. Except for the prism layers, the others are form by tetrahedral cells.

The number of cells will affect the calculated results, so the grid independence test is conducted (Wang and Wang 2016; TienPhuc *et al.* 2016). The criteria for selecting the number of cells is based on the  $Cd$ ,  $Cl$  corresponding to each number of cells, which is tabulated in Table 1. In order to ensure the boundary of the simulation keeping agreement with the experiment, the simulation is also conducted in non-crosswind condition. The velocity inlet boundary is used on the inlet and the velocity is -30m/s. Pressure-outlet boundary is used on the outlet. The top wall, sidewalls and floor are defined as no-slip walls. The results of experiment and simulation obtained from case 2 with a deviation of  $Cd$  and  $Cl$  is about 0.35% and 2.13% as shown in Table 1. The deviation of aerodynamic force coefficient between the wind tunnel test and simulation in the field of passenger car aerodynamics could be accepted. According to the simulation and experiment results and considering the computational resources, the case 2 is chosen in this study.

#### 4.1.3 Initial Condition

By preparing the initial condition of the coupled simulation, the passenger car in steady state without crosswind is simulated in the fluid dynamic. This simulation begins from the uniform pressure and velocity field and is terminated after 0.5s when the turbulent flow field around the passenger car develops.

#### 4.1.4 Experiment

To validate the simulation method, wind tunnel test is carried out in HD-2 Boundary Layer Wind Tunnel in Wind Engineering Research Center, Hunan University. The wind tunnel is a closed-circuit type wind tunnel, and it is composed by two closed test sections. The area of the high speed section is  $3 \times 2.5 \text{m}^2$ , and the length is 17m. The maximum wind speeds is 58 m/s. The 1/3-scale model is used in the test as shown in Fig 6(a). The measurements for the velocity fields in the near wake of the passenger car model were carried out by a commercial PIV, as shown in Fig 6(b). Which could record successive images of the 2D velocity in the flow field around the passenger car model. The PIV system is consisted of a double pulse laser, a data acquisition system and a CCD camera. The pulse energy of the double pulse laser is 500 *mJ/pulse* and the wavelength is 532*nm*. The CCD camera of  $4000 \times 2672$  pixels resolution records particle images, operated under a sampling rate of 5Hz.

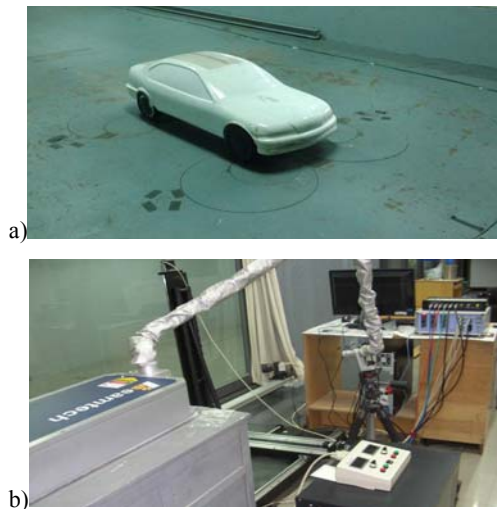


**Fig. 6. Experiment facilities: a) passenger car in wind tunnel; b) PIV system.**

Figure 7 shows the comparisons of the wake flow velocity contours between the experiment and simulation when the yaw angle of the passenger car is 0deg and 15deg. The structures of the wake flow field display good agreement between measured and simulated. Both of them have a pair of opposite revolving vortex at the tail of the passenger car. The height and length are also very similar. In conclusion, accuracy of CFD results paves the way for the calculation of flow field around the passenger car body.

#### 4.2 Vehicle Dynamics Simulation

The parameters value of the passenger car are listed in Table 2. The parameters of the passenger car, such as mass, and inertia moment, were given by characteristic of the commercial passenger car.

**Table 2 Main parameters for the passenger car**

Parameters	Values	Units
$m$	1299	kg
$l_f$	1.24	m
$l_r$	1.57	m
$I_z$	6022.4	kg·m <sup>2</sup>
$d$	1.53	m
$S$	2.053	m <sup>2</sup>

#### 4.3. Methodology

##### 4.3.1 Fully-Coupled Method

The schematic of numerical simulation data is transferred in fully-coupled simulation as shown in Fig. 8. The data exchange between the fluid dynamics simulation and vehicle dynamic simulation for each time step. At first, the aerodynamic loads are obtained at steady state. Then, the aerodynamic forces and moments are transferred to the vehicle dynamic model. The vehicle dynamic model calculates the motion of the passenger car and transfers the information of the

velocity to the fluid dynamic. The unsteady aerodynamic loads of the passenger car in the new position are calculated by the fluid dynamic. The next is repeating the preceding process. Since the position of the passenger car in the fluid dynamic is changed, the grid must be changed in this step. The dynamic mesh is used to re-mesh the grid in this study. Two types of meshing methods smoothing and re-meshing are used in this study.

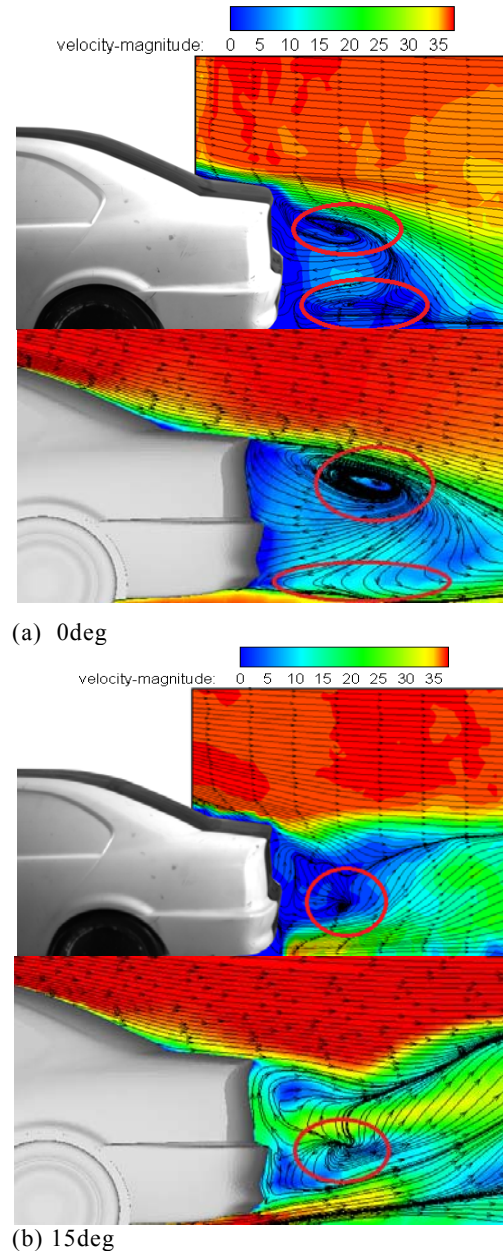


**Fig. 7. Comparison of velocity contours and the velocity streamlines between wind-tunnel measurement (top) and simulation (bottom) on Y=0 section.**

In order to ensure the simulation accuracy, the discretized time period is very important. If the discretized time period is set very small, the time of the simulation will be too long. If the discretized

time period is set very large, the accuracy of the simulation will be very poor. According to our computing resources, the discretized time period is set to  $5.0 \times 10^{-5}$ s in this study. The CFL number is around 0.9 throughout the whole flow.

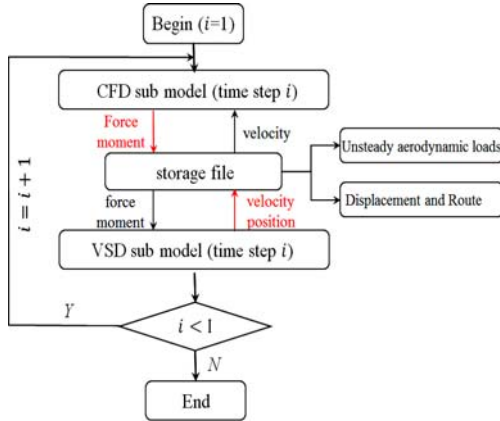


Fig. 8. Flow chart of fully-coupled method.

### 4.3.2 Quasi-Steady Method

In order to compare with the coupled method, transitional method based on a quasi-steady assumption, was adopted to evaluate the aerodynamics loads. The lateral force and yawing moment are expressed as

$$F_w = \frac{1}{2} C_s(\beta_w) \rho S V_r^2$$

$$M_w = \frac{1}{2} C_{ym}(\beta_w) \rho S l V_r^2$$

The coefficient of the lateral force and yawing moment can be obtained from the approximate polynomials of the yaw angle. The approximate polynomials is built on the results of several steady state. Based on the results of the steady simulation, the polynomials express as follow,

$$C_s(\beta_w) = 3 \times 10^{-8} \times \beta_w^5 - 4 \times 10^{-6} \times \beta_w^4 + 2 \times 10^{-4} \times \beta_w^3 + 0.0589 \times \beta_w - 0.0029$$

$$C_{ym}(\beta_w) = -1 \times 10^{-8} \times \beta_w^5 + 3 \times 10^{-6} \times \beta_w^4 - 2 \times 10^{-4} \times \beta_w^3 + 3.6 \times 10^{-3} \times \beta_w^2 + 8.6 \times 10^{-3} \times \beta_w + 0.0012$$

Figure 9 presents the results of the quasi-steady simulation and the approximate function.

### 4.3.3 One-Way Method

The other transitional simulation method is regarded as the one-way method. The process of the crosswind effect on passenger car's stability in one-way simulation is shown in Fig. 10. First, the flow field of the passenger car is simulated and the aerodynamic loads are obtained. Then, the aerodynamic loads are used on the vehicle dynamic model. As a result, the influence of the crosswind to the passenger car is considered, but the influence of the passenger car's attitude changes to the flow field are not considered.

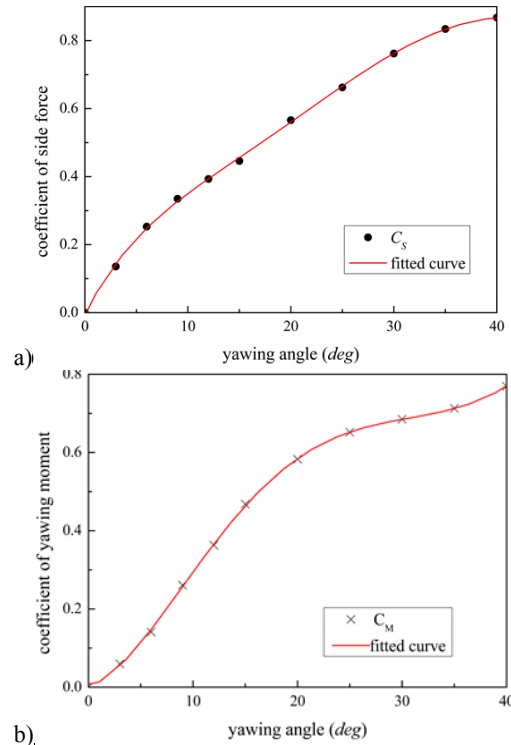


Fig. 9. Fitted curve of the coefficient aerodynamic loads. a) side force; b) yawing moment.

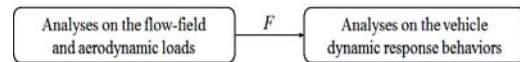


Fig. 10. Flow chart of one-way method.

For the coupling simulation of the unsteady aerodynamics and the passenger car motion, the Eqs. (1) – (7) for passenger car-fluid dynamic interactions are obtained. Equations (1) – (2) are solved by ANSYS Fluent. The fully-coupled simulation is conducted on the 64CPU and 128G memory. Because the vehicle back to the normal route needs some times, the driver should adjust the vehicle when the crosswind is disappeared. In order to study the change process of the vehicle and the aerodynamics characteristic in crosswind condition and non-crosswind condition, the fully-coupled simulation is set to 12.5s, which takes about 650h.

## 5. RESULTS AND DISCUSSION

In this section, the passenger car at a speed 30m/s in the “1-cos” cross wind is analyzed by fully-coupled methods, quasi-steady methods and one-way methods, as well as the interplay of the passenger car motion and the unsteady aerodynamics.

### 5.1 Coefficient of Aerodynamic Loads and Flow Field

The time series of the coefficient of aerodynamic loads are shown in Fig. 11, and the results of quasi-steady and one-way simulation are also shown in the figure.

The coefficient of side force in Fig. 11(a) shows similar profile between the three simulations. The side force increases when the crosswind is added and decreases when crosswind is disappeared. Nevertheless, there are some differences between the results of the three simulations. The coefficient of side force in the fully-coupled simulation is bigger than the other two methods when the crosswind is added and disappeared. In fully-coupled and one-way simulation, the change of the coefficient of side force is more obvious than the change of the coefficient of side force in quasi-steady simulation when the crosswind is added. The main reason to this phenomenon is the simulation methods are different in solving the fluid dynamic equations. The steady simulation method is adopted in quasi-steady simulation, and the transient simulation method is employed in fully-coupled and one-way simulation. In the crosswind region, the negative peak of the coefficient of side force is -0.96, -0.93 and -0.86 in fully-coupled simulation, one-way simulation and quasi-steady simulation, respectively. The negative peak in fully-coupled simulation is about 1.03 times than in one-way simulation and 1.12 times than in quasi-steady simulation. In the quasi-steady and on-way simulation, the coefficient of side force quickly reaches to steady state when the crosswind is vanished. However, the coefficient of side force can't reach to steady state in fully-coupled simulation when the crosswind is vanished due to the effect of the passenger car motion and the hysteresis effect of the flow field (Krajnovic *et al.* 2011; Gu *et al.* 2016).

moment in Fig. 11(b) also have similar profile between the three methods. But the difference between the quasi-steady simulation and the fully-coupled and one-way simulation is very obvious. The coefficient of yawing moment has positive and negative peak values in fully-coupled and one-way simulation when the crosswind is just added and vanished, and the positive and negative values in the two methods are about 0.32 and -0.90, respectively. However, there is not obvious positive and negative peak values in quasi-steady simulation. The main reason is that the steady simulation method is used in quasi-steady simulation, which can't reflect the hysteresis effect of the flow-field to the aerodynamic force. The peaks are caused by the flow-field around the passenger car which is changing in a short time, and the hysteresis effects of the flow field have some influence to the aerodynamic loads. However, the difference of the coefficient of yawing moment between the fully-coupled simulation and the one-way and quasi-steady simulation is also obvious when in crosswind is vanished. The coefficient of yawing moment quickly reaches the steady state in one-way and quasi-steady simulation, but in fully-coupled simulation can't quickly reaches the steady state, which is the same as the change of coefficient of side force.

Regarding the lateral motion and the driver's reaction, the side force and yawing moment exhibit transitional behaviors when the crosswind is added and disappeared, and the influence to the flow-field will be shown in next section. Hence, their effects on vehicle dynamics should be considered when the vehicle driving on road. The main reason to the transitional behaviors is the change of the flow field around the vehicle. The flow field around the vehicle become very unstable when the crosswind is added and disappeared. The unstable flow filed will cause the fluctuation of the side force and yawing moment.

In order to understand the physical mechanisms of the unsteady loads shown in the previous, the flow around the passenger car is visualized from the simulation results. In this section, the surface pressure and flow-field are discussed. According to the change of the aerodynamic load and the vehicle motion route, six different moments are select as shown in Figs. 12 and 13. Fig. 12 presents snapshots of the pressure-coefficient distribution on the lateral surface of the passenger car. Fig. 13 exhibits the pressure and velocity field around the passenger car. Both figures are given at selected typical instances from  $t=0.30s$  to  $t=5.05s$ .

In the non-crosswind condition at  $t=0.30s$ , with the pressure distribution on the surface of the passenger car, the pressure field and velocity field are almost symmetric. When the passenger car subjected to the crosswind at  $t=1.39s$ , the change of the flow field around the passenger car is obviously. A large separation area is observed on the leeward. The pressure distribution on lateral side is quite different, and the direction of wake flow also has obvious changes. The course deviation is not apparent because the passenger car subject to the crosswind for a short time. At  $t=2.45s$ , when the

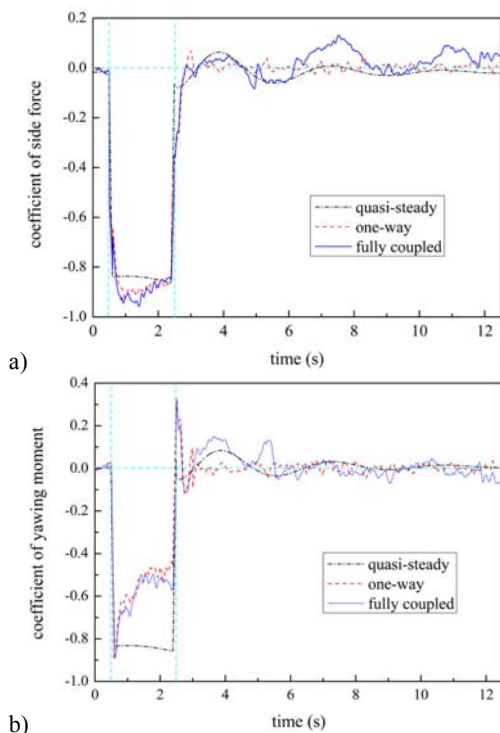


**Fig. 11. a) Coefficient of side force; b) coefficient of yawing moment.**

On the other hand, the coefficient of yawing

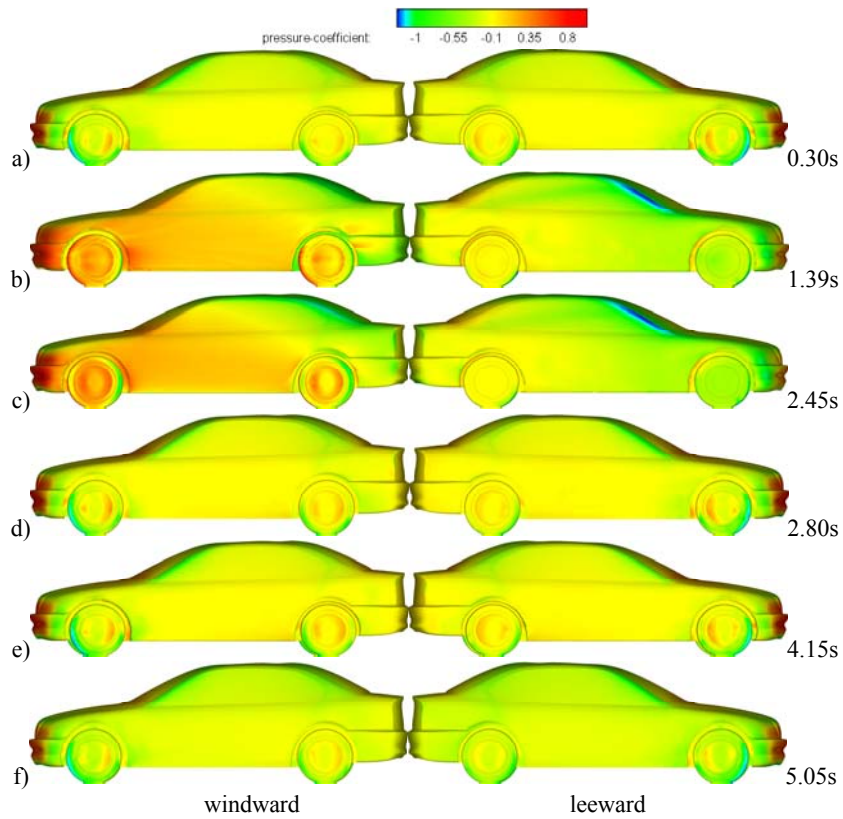


**Fig. 12. Pressure-coefficient distribution on lateral surface of passenger car.**

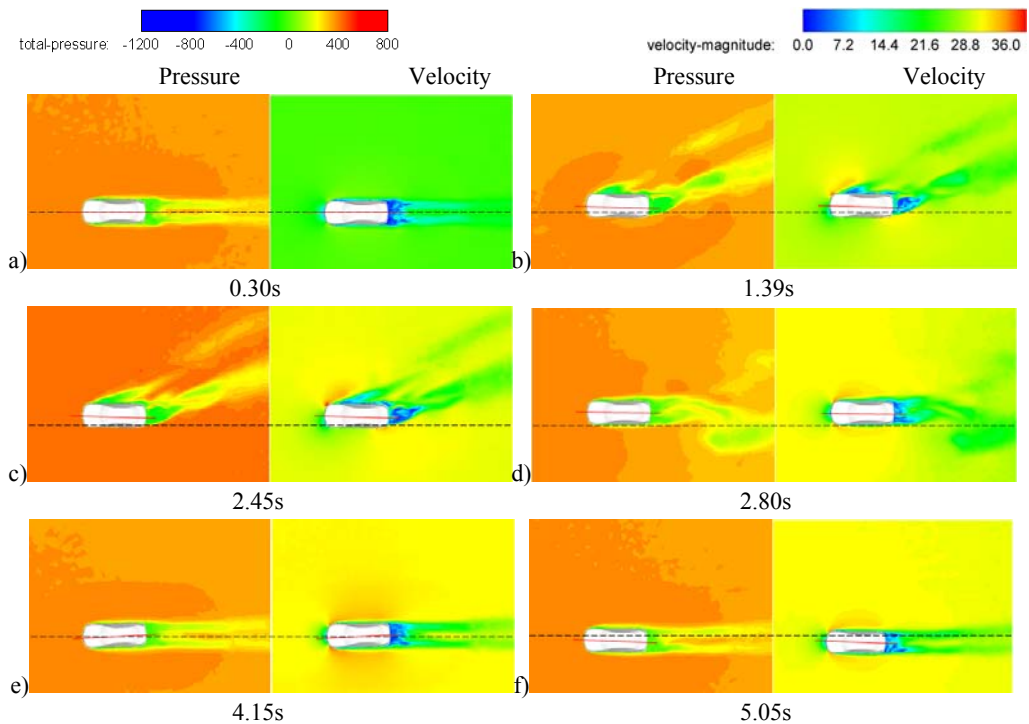


**Fig. 13. Flow velocity (right) and pressure (left) under the passenger car on XY-section ( $z=700\text{mm}$ ).**

coefficient of the yawing moment is on the positive peak. The course deviation is very obviously, and there is apparent change of the flow field around the

passenger car. The pressure distribution on both side of lateral surface are quite different. There is large area of positive pressure on the windward, and

the negative pressure is distributed widespread on the leeward. The flow field around the passenger car is obviously asymmetric, e.g., a large separation area is appeared on the rear end. At  $t=2.80s$ , there is not apparent change of the flow field around the passenger car due to the crosswind is disappeared. The difference of the pressure distribution on the lateral side is not obvious, and pressure and velocity field recovers its symmetrical property. The tiny asymmetric of the flow field is caused by the lateral velocity of the passenger car. At  $t=4.15s$ , the course deviation is equal to  $0m$ . The pressure distribution on lateral surface shows little difference. The flow around the passenger car also has some difference, especially at the rear of the passenger car. At  $t=5.05s$ , the lateral displacement is equal to  $0mm$ . The change of pressure distribution and flow filed around the passenger car is similar to position  $t=4.15s$  and  $t=5.05s$ , but there is some difference due to different lateral motion velocity.

Based on the time variations of the pressure distributions and the flow-filed, the change behaviors of the unsteady aerodynamic loads can be understood, as mentioned in the previous.

### 5.2 Passenger Car Motion

The time series of the lateral displacement and yaw angle in the three methods are presented in Fig. 14. The results of the fully coupled simulation, quasi-steady and one-way simulations show obvious difference, especially in yaw angle when the passenger car subjected to the crosswind. In the fully-coupled analysis, the lateral displacement starts to increase when the crosswind is added around  $t=0.50s$ , and the passenger car begin to leave the original track. The lateral displacement continues to increase until  $t=2.80s$ , and the displacement reaches to the negative peak which value is  $0.64m$ . The change of the displacement shows fluctuation, and the displacement is gradually decrease until stability.

The yaw angle is changed due to the driver's action. The change rule shows in fluctuation, but there is distinct difference between the change of the yaw angle and the change of the lateral displacement in the fully-coupled simulation. The yaw angle also starts to increase when the crosswind is added at  $t=0.50s$ , and reaches to a negative peak at  $t=1.40s$ . The positive peak value is  $0.35rad$  at  $t=4.01s$ , and the negative peak value is  $-0.24rad$  at  $t=5.50s$ .

The difference of the lateral displacement is obviously between the three methods as shown in Fig. 14(a). Although the negative peak of lateral displacement almost appears at the same time  $t=3.0s$ , the peak value have some differences. The negative peak value with steady aerodynamic load is bigger than the value with unsteady aerodynamic load. The negative value in fully-coupled, one-way, quasi-steady simulation is  $-0.62m$ ,  $-0.68m$  and  $-0.72m$ , respectively. After  $t=3s$ , the change of the lateral displacement between the three methods are also very obvious. Although the lateral displacement is fluctuating, and the fluctuation of the lateral displacement reaches to steady with steady aerodynamic load is quicker than with

unsteady aerodynamic load. The positive and negative peak value with the unsteady aerodynamic load is bigger than the value with the steady aerodynamic loads. In the quasi-steady and one-way simulation, the change of the lateral displacement is quite similar when the crosswind is disappeared, but there is some difference due to the different aerodynamic loads in the two methods.

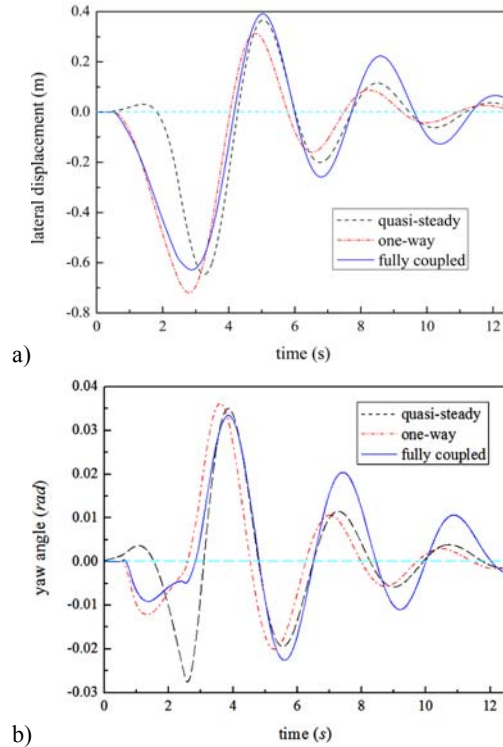


**Fig. 14. a)lateral displacement; b) yaw angle.**

The yaw angle of the passenger car predicted in the three methods are plotted in Fig. 14(b). There are many differences of the yaw angle between the three methods. The change rule of the yaw angle is more complicated than the change rule of the lateral displacement due to the driver's action and aerodynamic loads. The difference is particularly remarkable when the crosswind is added. The direction of the yaw angle is completely opposite around  $t=0.5$  between the quasi-steady simulation and one-way and fully-coupled simulation. This difference is induced by different behavior of the yawing moment as shown in Fig. 13(b). Because of the influence of the aerodynamics loads, the peak value of the yawing velocity in quasi-steady simulation is bigger than in one-way and fully-coupled simulation when the crosswind is added, and the peak value of the yaw angle in quasi-steady, one-way and fully-coupled simulation is  $0.28rad$ ,  $0.13rad$  and  $0.09rad$ , respectively. The fluctuation of yaw angle with the steady aerodynamics is smaller than with unsteady aerodynamic loads when the crosswind is disappeared. The main reason to this phenomenon is the change of the unsteady aerodynamic loads. Fig. 11 presents that the coefficient of the yawing moment and side force

have large difference between the three methods when crosswind is not exist. This difference is caused by the flow field around passenger car which is influenced by the change of the passenger car's posture and the hysteresis effect of the flow.

From the above discussion could be found that the unsteady aerodynamics affects enough to the yawing motion and trajectory of the passenger car. On the other hand, it is very important to precisely control and judge the course of a passenger car when subjected to crosswind.

### 5.3 Drivability of the Passenger Car

In order to estimate the stability and drivability of the road passenger car, there are many index parameters, and the yaw angular velocity is the one of the most important parameters. Fig. 15(a) shows the yaw angular velocity. The difference of the yaw angular velocity between the three methods are very obviously. During the crosswind is added, the difference of the yaw angular velocity between the quasi-steady simulation and the one-way and fully-coupled simulation is very apparent. The change rule of the yaw angular in quasi-steady simulation is completely opposite to the change rule in one-way and fully-coupled simulation. The nagtive peak value of the one-way and fully-coupled simulation is appeared around  $t=0.8s$ , and in the quasi-steady simulation is around  $t=2.50s$ . However, the yaw angular velocity with the steady aerodynamic loads reach to the steady state faster than with the unsteady aerodynamic loads.

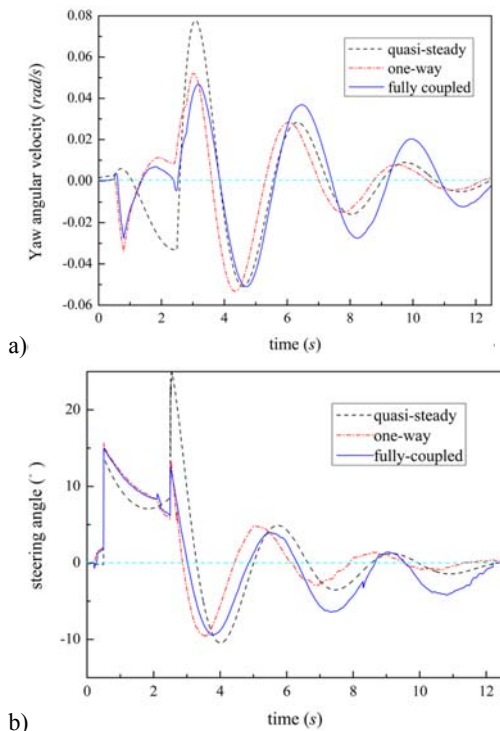


**Fig. 15. a) yaw angular velocity; b) steering angle.**

The amplitude of the steering wheel angles is also regarded as a parameter closely related to the human reaction of the running stability and

drivability in crosswinds condition. Fig. 15(b) plots the steering angle in the three methods. Distinct difference of the steering angle can be observed between the three methods. The major difference is the positive peak value between the three simulations, and the peak value in quasi-steady simulation is bigger than in one-way and fully-coupled simulation. These difference shows the effects of the unsteady aerodynamics is very important to the stability and drivability of a passenger car when subjected to crosswind.

It should be note that the change of the crosswind is very complicated in nature, and its' influence to the vehicle is also very complicated. Therefore, the crosswind should be investigated more realistic in the future. The vehilce drives in and out of a crosswind area which is not considered in this study, and the change of unsteady aerodynamics is very remarkable at this moment, which should be studied in the future. The other parameters related to the vehicle drivability and stability should be investigated in more accurate vehicle model in next study.

## 6. CONCLUSION

An investigation of unsteady aerodynamic of a passenger car in “1-cos” crosswind coupled with passenger car motion have been performed in this study, which employs the fully-coupled, quasi-steady and one-way simulation methods are employed. For the vehicle dynamics simulation, the passenger car is simplified as a 3 DOF system and the driver's control is considered. In the aerodynamics simulation, Large eddy simulation with dynamics mesh techniques is adopted to simulate the transient flow-field around the passenger car. In quasi-steady and one-way simulation, the aerodynamic loads are obtained firstly and applied on the vehicle dynamics model. However, the aerodynamic loads is obtained as the passenger car motion in fully-coupled simulation. The result of fully-coupled method is more similar to reality than the result of the quasi-steady and one-way simulation.

The results of the fully-coupled, quasi-steady and one-way simulation indicate that unsteady aerodynamics loads have significant influences to the passenger car motion of the passenger car. Large difference could be found by comparison of the results of the three methods. The peak of the lateral displacement in fully-coupled simulation is smaller than in quasi-steady or one-way simulation, the peak vaule in fully-coupled, one-way, quasi-steady simulation is 0.62m, 0.68m and 0.72m, respectively. The change tendency of the lateral force, yaw angle, yaw angular velocity and steering angle in quasi-steady simulation is quite different with the change tendency in fully-coupled and one-way simulation, due to the different simulation solver adopted. Because the hysteresis effect of the flow, the change of results of the fully-coupled simulation is more obviously than one-way and quasi-steady simulation. These results clearly indicated the importance of the unsteady

aerodynamic in moving analysis of passenger car.

### ACKNOWLEDGMENTS

This work is supported by Key Project in the Science and Technology Program of Changsha, China (K1501011-11), National Automotive High Level Independent Innovation Program of China, National Hundred, Thousand, and Ten Thousand Talent Program of Ministry of Transport of China (Grant No.20120222), Independent Subject of State Key Laboratory of China (Grant No.734215002), and Innovation Team of Ministry of Finance of China (Grant No.04200036017), National Nature Science Foundation of China (Grant No.51305312).

### REFERENCES

- Baker, C. J. (1988). High sided articulated road vehicles in strong cross winds. *J. Wind Eng. Ind. Aerodyn.* 31(1), 67-85.
- Bakker, E, H. B. Pacejka and L. Lidner (1989). A new tire model with an application in vehicle dynamics studies. *SAE paper*.
- Cai, C. S., J. Hu, S. Chen, Y. Han, W. Zhang and X. Kong (2015). A coupled wind-vehicle-bridge system and its applications: a review. *Wind Struct* 20(2), 117-142.
- Carrarini, A. (2007). Reliability based analysis of the crosswind stability of railway vehicles. *J. Wind Eng. Ind. Aerodyn.* 95(7), 493-509.
- Chu, C., C. Chang, C. Huang, T. Wu, C. Wang and M. Liu (2013). Windbreak protection for road vehicles against crosswind. *J. Wind Eng. Ind. Aerodyn.* 116(5), 61-69.
- Cui, T., W. Zhang and B. Sun (2014). Investigation of train safety domain in cross wind in respect of attitude change. *J. Wind Eng. Ind. Aerodyn.* 130, 75-87.
- Gu, Z. Q., T. M. Huang, Z. Chen, Y. Q. Zong and W. Zeng (2016). large eddy simulation of the flow-field around road vehicle subjected to pitching motion. *J. Appl. Fluid Mech.* 9(6), 2731-2741
- Gulyasa, A., A. Bodorb, T. Regertb and I. M. Jánosic (2013). PIV measurement of the flow past a generic car body with wheels at LES applicable Reynolds number. *J. Heat Fluid Flow* 43, 220-232
- Hucho, W. and G. Sovran (1993). Aerodynamics of road vehicles. *Annual Reviews of Fluid Mechanics* 25, 485-537
- Jonathan, M., F. Erik, R. Gregory, K. Rajan, T. Kunihiko, A. Farrukh, Y. Yoshihiro and M. Kei (2015). Drag reduction on a flat-back ground vehicle with active flow control. *J. Wind Eng. Ind. Aerodyn.* 145, 292-303
- Krajnovic, S., A. Bengtsson and B. Basara (2011). Large eddy simulation investigation of the hysteresis effects in the flow around an oscillating ground vehicle. *ASME: J. Fluids Eng.* 133(12).
- Li, Y. L., P. Hu and Y. L. Xu (2014). Wind loads on a moving vehicle-bridge deck system by wind-tunnel model test. *Wind and Structures* 19(2), 145-167
- Liu, Z., T. Ishihara, X. He, H. Niu (2016). LES study on the turbulent flow fields over complex terrain covered by vegetation canopy. *J. Wind Eng. Ind. Aerodyn.* 155, 60-73.
- Mitschke, M. and H. Wallentowitz (2004). *Dynamik der kraftfahrzeuge*. Springer-Verlag.
- Maruyama, Y. and F. Yamazaki (2006). Driving simulator experiment on the moving stability of an automobile under strong crosswind. *J. Wind Eng. Ind. Aerodyn.* 94(4), 191-205.
- Nakashima, T., M. Tsubokura, M. Vazquez and *et al* (2013). Coupled analysis of unsteady aerodynamics and vehicle motion of a road vehicle in windy conditions. *Comput Fluids* 80, 1-9.
- Nakashima, T., M. Tsubokura, S. Matsuda and Y. Doi (2011). Unsteady Aerodynamics Simulation of a Heavy-Duty Truck in Wind Gusts Coupled With Vehicle Motion Analysis in Six Degrees of Freedom. In *Proceeding of Asme-jsme-ksme Joint Fluids Engineering Conference* 1013-1024.
- Okada, Y., T. Nouzawa, T. Nakamura and S. Okamoto (2009). Flow structures above the trunk deck of sedan-type vehicles and their influence on high-speed vehicle stability 1st report: on-road and wind-tunnel studies on unsteady flow characteristics that stabilize vehicle behavior. *SAE paper*.
- Osth, J. and S. Krajnović (2014). A study of the aerodynamics of a generic container freight wagon using Large-Eddy Simulation. *J. Fluid Struct.* 44, 31-51.
- TienPhuc, D, G. ZhengQi and C. Zhen (2016). Numerical simulation of the flow field around generic formula one. *J. Appl. Fluid Mech.* 9(1), 443-450
- Tosolin, G., J. Webb, A. Catala, A. Escuer, Y. J. Hyun (2012). Development of methodologies for evaluation, simulation and improvement of cross-wind sensitivity. In *Proceedings of the FISITA 2012 World Automotive Congress*, Springer Berlin Heidelberg 23-33.
- Uystepruyst, D. and S. Krajnovic (2013). LES of the flow around several cuboids in a row. *J. Heat Fluid Flow* 44, 414-424
- Wang, B (2014). Crosswind Effects on Road Vehicles Moving on Ground and Long-Span Bridges. Ph. D. thesis, The Hong Kong Polytechnic University.
- Wang, B., Y. L. Xu (2015). Safety analysis of a road vehicle passing by a bridge tower under crosswinds. *J. Wind Eng. Ind. Aerodyn.* 137, 25-36

- Wang, J. S. and C. Wang (2016). Heat transfer and flow characteristics of a rectangular channel with a small circular cylinder having slit-vent vortex generator. *Int. J. Therm. Sci.* 104, 158-171
- Wang, Y., Y. Xin, Z. Gu, S. Wang, Y. Deng and X. Yang (2014). Numerical and experimental investigations on the aerodynamic characteristic of three typical passenger vehicles. *J. Appl. Fluid Mech.* 7(4), 659-671
- Zhou, Y., and S. Chen (2015). Fully coupled driving safety analysis of moving traffic on long-span bridges subjected to crosswind. *J. Wind Eng. Ind. Aerodyn.* 143, 1-18
- Zhu, Z. W. (2015). LES prediction of aerodynamics and coherence analysis of fluctuating pressure on box girders of long-span bridges. *Comput Fluids* 110(30), 169-180